Biofuel Research Journal 41 (2024) 2013-2024

Biofuel Research Journal

Journal homepage: www.biofueljournal.com

Original Research Paper

Artificial humic substances as sustainable carriers for manganese: Development of a novel bio-based microfertilizer

Alexander Volikov[1,*], Helen Schneider[1], Nadezda V. Tarakina[1], Nader Marzban[2], Markus Antonietti[1], Svitlana Filonenko[1]

[1]*Max Planck Institute of Colloids and Interfaces, Potsdam Science Park, Am Mühlenberg 1, 14476, Potsdam, Germany.*

[2]*Leibniz Institute for Agricultural Engineering and Bio-economy e.V. (ATB), Max-Eyth- Allee 100, 14469 Potsdam, Germany.*

HIGHLIGHTS

- Sustainable manganese fertilizer with artificial humic substances (AHS) was produced.
- Manganese could bind to a high-molecular-weight fraction of AHS.
- The addition of manganese minimally could alter the structure of AHS.
- Manganese in AHS was predominantly in amorphous Mn(II) bioavailable form.
- Manganese-rich AHS increased manganese uptake by up to 64 mg/kg in dry cucumber biomass.

GRAPHICAL ABSTRACT

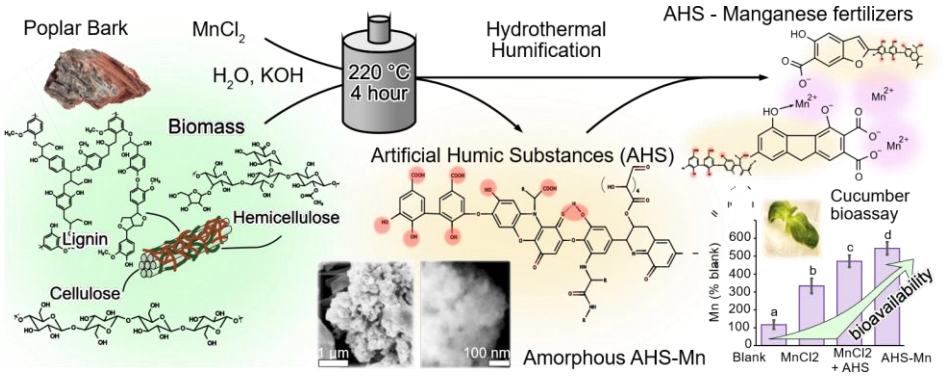

ARTICLE INFO

Article history:
Received 27 January 2024
Received in revised form 23 February 2024
Accepted 23 February 2024
Published 1 March 2024

Keywords:
Humic
Manganese
Fertilizer
Hydrothermal
Humification
Poplar bark

ABSTRACT

This study presents a new strategy for the production of sustainable manganese fertilizer based on artificial humic substances (AHS). AHS with different manganese concentrations (0–20%) were synthesized from poplar bark under alkaline conditions *via* hydrothermal treatment. For the 20% manganese formulation, the interaction of manganese with AHS resulted in reduced solubility (from 25.2% to 12.3% organic carbon) and average molecular weight of humic acids (from 11.6 to 3.9 KDa), indicating preferential binding of the high-molecular-weight fraction. The formulation with 5% of manganese achieved optimal manganese loading without compromising the AHS solubility (19.4%). Structural analyses showed only minor changes in AHS in the presence of manganese, indicating that the main structural fragments of the AHS were preserved. Structural, morphological, and spectroscopic characterizations confirmed the formation of amorphous manganese complexes within the AHS matrix, primarily in the plant-available Mn(II) oxidation state. Plant bioassays showed increased manganese uptake with the application of AHS containing 5% Mn compared to $MnCl_2$ alone (64 mg/kg *vs*. 40 mg/kg in dry cucumber biomass). Interestingly, unmodified AHS at higher concentrations (50 mg/L) further enhanced manganese (67 mg/kg) and iron (up to 209 mg/kg) uptake, highlighting the potential role of AHS in facilitating metal transport.

* Corresponding author at:
E-mail address: Alexander.Volikov@mpikg.mpg.de

Please cite this article as: Volikov A., Schneider H., Tarakina N.V., Marzban N., Antonietti M., Filonenko S. Artificial humic substances as sustainable carriers for manganese: Development of a novel bio-based microfertilizer. Biofuel Research Journal 41(2024) 2013-2024. DOI: 10.18331/BRJ2024.11.1.3.

Contents

Abbreviations

ADF-STEM	Annular dark-field scanning transmission electron microscope
AHS	Artificial humic substances
AHS-Mn	Manganese-rich artificial humic substances
ANOVA	Analysis of variance
DMSO	Dimethyl sulfoxide
EDTA	Ethylenediaminetetraacetic acid
EDX	Energy dispersive X-ray
EEL	Electron energy loss
FA	Fulvic acids
FTIR	Fourier-transform infrared
GPC	Gel permeation chromatography
HA	Humic acids
HPLC	High-performance liquid chromatography
HS	Humic substances
HSQC	Heteronuclear single quantum coherence
IUPAC	International union of pure and applied chemistry
NMR	Nuclear magnetic resonance
PTFE	Polytetrafluoroethylene
SEM	Scanning electron microscopy
SPE	Solid-phase extraction
STEM	Scanning transmission electron microscopy
TOC	Total organic carbon
XRD	X-Ray powder diffraction

1. Introduction

Micronutrients such as zinc, iron, and manganese are essential for plant growth and development, although they are required in trace amounts (Saquee et al., 2023). The increasing prevalence of micronutrient deficiencies in agricultural soils poses a formidable challenge to global food production and security (Dimkpa and Bindraban, 2016). These deficiencies result from a number of factors, including intensive agricultural practices, soil erosion, and an over-reliance on fertilizers that focus on macronutrients (nitrogen, phosphorus, and potassium) (Gupta, 2005). Micronutrient-deficient soils directly limit crop yields by inhibiting plant development and reducing resistance to environmental stresses (Hajiboland, 2012). Critically, micronutrient deficiencies extend beyond crop yield and profoundly affect the nutritional quality of crops. Plants grown in deficient soils have lower concentrations of essential micronutrients. This issue directly translates into reduced nutritional value in human diets, exacerbating the "hidden hunger" of widespread micronutrient deficiencies that plague the world's population (Nieder et al., 2018; Chakraborty et al., 2021).

Manganese, despite being needed in small quantities, is among the most crucial micronutrients, typically required at levels of 10–20 mg/kg (Broadley et al., 2012), exerts a significant influence on plant physiology (Alejandro et al., 2020). It serves as a critical cofactor in photosynthesis, particularly in the oxygen evolution complex of photosystem II, and activates numerous enzymes involved in plant metabolism (Andresen et al., 2018; Schmidt and Husted, 2019). Inadequate manganese availability may result in chlorosis, manifested as yellowing between the leaf veins while the veins remain green, with hallmark symptoms such as necrotic spots and stunted growth that may also occur, particularly in younger leaves (Rashed et al., 2021). Nevertheless, even though required in small quantities, a decrease in manganese levels can significantly impact biomass and disrupt vital plant functions, such as tolerance to low temperatures (Alejandro et al., 2020). Correcting manganese deficiency is essential for optimal plant health and productivity. Main strategies include modifying soil pH to increase Mn solubility, seed treatment as one of the most costless, foliar applications of manganese fertilizers for rapid uptake, and usage of manganese-enriched fertilizers (Reuter et al., 1988).

Two primary categories of Mn fertilizers are used to address manganese deficiencies in agricultural soils: manganese salts or oxides and chelates (Khoshru et al., 2023). The most commonly used manganese fertilizer in global crop production is manganese sulfate (Alloway, 2008). It offers a cost-effective solution, excellent water solubility, and quick availability. However, it may be prone to soil interactions and potential leaching. Chelates, such as complexes of Mn with EDTA, form stable structures that protect Mn from direct soil interactions (López-Rayo et al., 2014). Chelates typically demonstrate enhanced mobility and uptake by plants, albeit at a higher cost. However, they can face challenges such as potential manganese displacement by other soil elements, like iron, which can form stronger complexes with the most common chelate, EDTA (Norvell and Lindsay, 1969). While conventional water-soluble manganese fertilizers are valuable, they are susceptible to drawbacks such as potential leaching, especially in sandy, acidic, or over-watered soils (Rashed et al., 2021). This issue can lead to the rapid movement of metals below the root zone, hindering plant uptake and posing a risk of groundwater contamination.

Soil is a dynamic system in which essential micronutrients such as iron, zinc, and manganese undergo complex interactions that affect their availability to plants (Rengel, 2015). Mineral complexation and chelation are two key mechanisms that control micronutrient transport within the soil (Boiteau et al., 2018; Dhaliwal et al., 2023). These processes involve the formation of bonds between micronutrients and other molecules, thus increasing their solubility. Soil organic matter, consisting primarily of humic substances (HS), plays a pivotal role in soil-related interactions (Dhaliwal et al., 2023). HS are complex supramolecular assemblies resulting from abiotic and biotic transformations of plant-derived biomacromolecules and other organic residues (MacCarthy, 2001). HS are heterogeneous, high-molecular-weight compounds with numerous functional groups that readily complex and chelate micronutrients. These interactions enhance micronutrient solubility, decrease their vulnerability to immobilization, and ultimately facilitate their uptake by plants (Zanin et al., 2019).

Humic-based fertilizers use the benefits of these natural processes to optimize micronutrient delivery. They offer several advantages over traditional mineral fertilizers. HS-complexed micronutrients exhibit increased solubility and protection from soil reactions that often render them unavailable to plants (Chen, 1996). HS act as a natural reservoir, gradually releasing micronutrients as they decompose, ensuring a sustained supply that matches plant needs (Ampong et al., 2022). HS positively impact soil structure, water-holding capacity, and microbial activity, contributing to a

Please cite this article as: Volikov A., Schneider H., Tarakina N.V., Marzban N., Antonietti M., Filonenko S. Artificial humic substances as sustainable carriers for manganese: Development of a novel bio-based microfertilizer. Biofuel Research Journal 41 (2024) 2013-2024. DOI: 10.18331/BRJ2024.11.1.3.

healthier soil environment conducive to nutrient cycling and uptake (Lumactud et al., 2022). Several studies have demonstrated the potential for obtaining new fertilizers based on HS through the use of chelate and other properties to transport iron (Sorkina et al., 2014; Cieschi et al., 2019). These works propose the use of synthetic iron humates, which have been shown to have a positive effect on correcting iron deficiency in plants. Similar approaches can be applied to manganese, which behaves similarly to iron in nature.

Artificial Humic Substances (AHS) are emerging as a sustainable and versatile tool to address the challenges of modern agriculture (Yang and Antonietti, 2020; Yang et al., 2023). These substances, synthesized through the hydrothermal conversion of biomass, mimic the properties and functionalities of natural HS. With clear advantages in biomass processing and targeted applications, AHS hold great promise for improving agricultural efficiency and sustainability - a potential recognized by IUPAC in its recent "Top Ten Emerging Technologies" list (Gomollón-Bel, 2021). Such tailor-made synthesis provides a high degree of control over the final properties of AHS, in contrast to the variability often found in natural sources. The similarity in functional groups between AHS and their natural counterparts suggests a comparable ability to facilitate micronutrient transport and accumulation in the soil. Furthermore, AHS synthesis allows for the targeted incorporation of essential elements, ushering in a new era of tailored microfertilizers.

This work presents a novel strategy for the synthesis of AHS-based microfertilizers. The integration of micronutrients during AHS synthesis offers the potential to create amorphous, bioavailable fertilizers. This approach leverages the established benefits of HS-based fertilizers, particularly their chelating properties, while enabling the development of customized nutrient delivery systems. By harnessing the potential of AHS, this method paves the way for optimizing agricultural production, improving soil health, and reducing reliance on unsustainable fertilization practices.

2. Materials and Methods

2.1. Synthesis of manganese-rich artificial humic substances

Poplar bark was used to produce artificial HS. All chemicals were purchased from Sigma-Aldrich and used as received. Deionized water (Evoqua GmbH, Barsbuttel, Germany) was used to prepare water solutions. The bark was first ground in a laboratory mill to a particle size of 0.1–1 mm. Then, mixtures of 3.6 mL water and 1.2 g bark with different amounts of KOH and $MnCl_2{\cdot}4H_2O$ were prepared. Four different mixtures were prepared with varying manganese contents of 1%, 5%, 10%, and 20% of biomass weight, and one control mixture without manganese. The corresponding preparations were named AHS for the mixture without manganese and AHS-MnX for the mixtures with manganese, where X corresponds to the manganese content. The KOH amount was calculated so that the pH value was neutral at the end of the reaction and with adjustments for the formation of manganese hydroxide. The amounts of KOH added were 0.2, 0.22, 0.3, 0.35, and 0.4 g for AHS, AHS-Mn1, AHS-Mn5, AHS-Mn10, and AHS-Mn20, respectively. The reaction mixtures were transferred into 50 mL pressure vessels with removable polytetrafluoroethylene (PTFE) cups from Parr (Moline, IL, USA). The hydrothermal process was carried out in an oven for 4 h after reaching 220 ℃. After the end of the reaction time, the autoclaves were taken out from the oven and kept at room temperature until cooled down to 25 ℃. After opening the autoclaves, the obtained slurries were transferred into 50-mL centrifuge tubes and centrifuged at 9000 rpm for 10 min (Hettich Universal320, Tuttlingen, Germany). The resulting solid and liquid fractions were analyzed after decantation.

2.2. Humic and fulvic acid separation and isolation

The liquid fraction of AHS was transferred to a beaker, and its pH was adjusted to 1.5 using 1 M HCl while stirring. This solution was centrifuged (9000 rpm, 10 min). The supernatant containing fulvic acids (FA) was decanted, and the precipitate humic acids (HA) was transferred to a 3.5 kDa cellulose membrane and dialyzed against deionized water until the solution resistance decreased below 0.1 µS. Then, HA were lyophilized (24 h, LYOTECH GT2-E benchtop freeze dryer) and collected. FA extraction was performed using a Bond Elut PPL cartridge (Agilent, USA, 200 mg sorbent). The cartridge was activated with 5 mL of methanol. Subsequently, 2 mL of deionized water was passed through the cartridge to remove the methanol, followed by the previously obtained FA solution. The cartridge was then washed with 5 mL of 0.01 M HCl to completely eliminate salts and dried under an air stream. The resultant FA were eluted with 10 mL of methanol and evaporated on a rotary evaporator.

2.3. Characterization of manganese-rich artificial humic substances

Carboxyl group content determination. The calcium acetate potentiometric titration method was used (Jeong et al., 2007). An accurately weighted sample of solid AHS ~ 20 mg was placed in 50 mL polypropylene centrifuge tubes. Deionized water (20 mL) was added, followed by 20 mL of a calcium acetate solution (~0.25 M). The mixture was agitated continuously for 24 h using an overhead stirrer. Subsequently, the mixture was centrifuged (9,000 rpm, 20 min), and the supernatant was filtered through a 0.45 µm PTFE membrane. Potentiometric titration of the released acetic acid within a 10 mL filtrate aliquot was performed using a standardized NaOH solution (0.02 M). To correct for potential hydrolysis of $Ca(OAc)_2$ during titration, a control titration was conducted using a solution of $Ca(OAc)_2$ in the absence of HA. The titration curve's equivalence point was determined through differentiation. The amount of carboxyl groups (mmol/g) was calculated using the following equation (**Eq. 1**).

$$C_{COOH} = C_{NaOH} \cdot \frac{(V_{NaOH} - V_0)}{m} \quad \text{Eq. 1}$$

where: V_{NaOH} - volume of NaOH solution required for titration of released acetic acid (mL), V_0 - volume of NaOH solution required for titration of $Ca(AcO)_2$ in the control experiment (mL), C_{NaOH} - concentration of the NaOH solution (mM), m - Mass of the sample in the aliquot (g).

- Fourier-transform infrared spectroscopy (FTIR)

FTIR measurements were performed using a Nicolet iS 5 FT-IR-spectrometer in conjunction with an iD5 ATR unit from Thermo Fisher Scientific. The spectra were recorded in the range 4000–400 cm^{-1} with 2 cm^{-1} resolution and 32 scans per sample and background.

- Nuclear-magnetic resonance (NMR) spectroscopy

All measurements were performed on an Agilent 400 MHz spectrometer (at 400 MHz for protons and 101 MHz for carbon-13). The solid lyophilized samples were dissolved in d-DMSO for the FA fraction and in 0.3M NaOD for the HA fraction at 5–7 wt% for analysis. ^{1}H NMR spectra were performed with a delay of 1 second and a collection of 128 scans. For 2D NMR spectra recording, the 1H-13C Multiplicity Edited Gradient HSQC method was used with a 2-second delay and a collection of 32 scans. The spectra were visualized and normalized using Mestrenova software.

- Total organic carbon (TOC)

An automatic carbon analyzer (TOC-L, Shimadzu, Japan) was used to quantify the organic and inorganic carbon content. The TOC content was determined by subtracting the inorganic carbon content from the total carbon content. To obtain statistically significant concentrations, multiple measurements were performed on each sample until a convergent result was obtained.

- Scanning electron microscopy (SEM)

The microstructure and chemical composition of obtained samples were analyzed using an LEO 1550-Gemini Zeiss scanning electron microscope equipped with an Oxford Instruments energy-dispersive X-ray (EDX) detector.

Please cite this article as: Volikov A., Schneider H., Tarakina N.V., Marzban N., Antonietti M., Filonenko S. Artificial humic substances as sustainable carriers for manganese: Development of a novel bio-based microfertilizer. Biofuel Research Journal 41 (2024) 2013-2024. DOI: 10.18331/BRJ2024.11.1.3.

- *Scanning transmission electron microscopy (STEM)*

For STEM observations, a suspension of the sample in ethanol was sonicated for 5 min and then drop-casted to the Au grid with lacey carbon support and dried for 15 min. The STEM study was performed using a double Cs-corrected JEOL JEM-ARM200F transmission electron microscopy operated at 80 kV and equipped with a cold-field emission gun and a high-angle silicon drift EDX detector (solid angle up to 0.98 steradians with a detection area of 100 mm^2) and a Gatan Quantum GIF spectroscopy system. Annular Dark Field Scanning Transmission Electron Microscopy (ADF-STEM) images and electron energy loss (EEL) spectra were collected at a probe convergence semi-angle of 25 mrad. EEL spectra were recorded in dual EELS mode at energy dispersions 0.1 eV/channel and 0.25 eV/channel, allowing correction for the zero-loss peak position. A power law model was used for the background subtraction. Multiple scattering effects have been removed using the Fourier ratio method, implemented in the Gatan Digital micrograph suite. The numerical smooth filter (low-pass parameter 1.0) was applied to the spectrum.

- *High-performance liquid chromatography (HPLC)*

Aromatics (phenols and furans) were quantified using an HPLC (Dionex ICS 3000; Thermo Fisher Scientific Inc., USA) equipped with a UV detector. Liquid samples were diluted (1:4) with 10% acetonitrile and filtered (0.2 µm PTFE, Neolab) prior to analysis. Organic acids (acetic, lactic, and formic) were measured using a UPLC system (Ultimate 3000) with a Eurokat H column and 0.01 N sulfuric acid mobile phase. Samples were diluted with deionized water (1:1). Extraction involved suspending 1 g of solid product in 40 mL of distilled water (60°C) with stirring (150 rpm, 40 min). The mixture was filtered (PTFE) and analyzed via HPLC and UPLC.

- *Gel permeation chromatography (GPC)*

GPC measurements were performed in phosphate buffer (0.067 M Na_2HPO_4) with 1 mL/min flow at 25 °C on an MCX-2 guard column in conjunction with an HS-PSS-MCX-analytical-5 µm-1000 column. The UV-vis signal was detected at 265 nm, and molecular weight was evaluated against a standard of polystyrene sulfonate sodium salt with molecular weight starting from 246 Da.

- *X-ray powder diffraction (XRD)*

Measurements were performed on a Rigaku SmartLab Powder Diffractometer with Cu Kα radiation. Match 3 software and the ICDD PDF-4+ crystallographic database (database version 4.2103) were used to detect crystalline phases (Gates-Rector and Blanton, 2019).

2.4. Bioassay

The bioassay experiments were carried out on cucumbers *Cucumis sativus L. cv.* "Salatgurken" as a target plant grown in modified Hoagland nutrient solution (Hoagland and Arnon, 1950) without manganese addition and prepared with deionized water of the following composition: 6 mM KNO_3, 4 mM $Ca(NO_3)_2$, 2 mM $MgSO_4$, 1 mM $NH_4H_2PO_4$, 46 µM H_3BO_3, 0.7 µM, $ZnSO_4{\cdot}7H_2O$, 0.3 µM $CuSO_4{\cdot}5H_2O$, 0.1 µM $Na_2MoO_4{\cdot}2H_2O$ and 15 µM Fe^{3+}–EDTA. Manganese is introduced in the form of an AHS-Mn5 sample or $MnCl_2{\cdot}4H_2O$ salt with 9.1 µM of metal concentrations. A total 6 series of solutions were prepared: blank - Hoagland nutrient solution without manganese; blank with addition of $MnCl_2{\cdot}4H_2O$; blank with addition of AHS (10 mg/L); blank with addition of AHS (10 mg/L) and $MnCl_2$; blank with addition of AHS (50 mg/L) and $MnCl_2{\cdot}4H_2O$ and blank with addition of AHS-Mn5. To simulate an alkaline soil environment, the pH of the solutions was adjusted to 8 using 0.1 M NaOH. The cucumber seeds were first germinated at 25°C in Petri dishes for 48 h in a solution of 0.5 mM $CaSO_4$ in deionized water and then transferred to glasses filled with 100 mL of nutrient solution. The seeds were grown using LED lamps (12-h light/12-h dark photoperiod; illumination, 40 µmol/m^2/s; 22 °C) for 7 days. After the test, the cucumber seedlings were washed with deionized water and then dried under vacuum at 40 °C. The content of manganese and iron was measured by Inductively Coupled Plasma Optical Emission Spectroscopy (ICP-OES Optima 8000) after oxidative digestion of the dried plants. For the studied parameters, the average value and standard deviation (SD) were calculated. Statistical data treatment was performed using the SciPy Python package version 1.12.0. One-way analysis of variance (ANOVA) was used to test for differences between average values.

3. Results and Discussion

3.1. Synthesis and general characteristics of manganese-rich artificial humic substances

In this study, we explore poplar bark as a renewable biomass resource. Poplar (*genus Populus*) is a fast-growing deciduous tree with significant applications in urban greening and carbon sequestration programs. Urban poplar provides ecosystem services, including dust and pollutant mitigation, soil stabilization, and hydrological regulation (Fortier et al., 2016). Moreover, these trees are potent carbon sinks; poplar plantations can sequester more than 10 tons of carbon annually per hectare (Fang et al., 2007). To prevent secondary carbon release, harvested poplar biomass – from urban removals, natural forests, or dedicated plantations – requires sustainable utilization options. While poplar wood finds applications in the paper, furniture, and cellulose-derivative industries, the bark poses processing challenges due to the bark's high lignin content and complex composition, which includes suberin, resins, fatty acids, flavonoids, condensed tannins, and various other components (Lupoi et al., 2015; Vangeel et al., 2023). We propose artificial humification *via* hydrothermal treatment as a strategy for valorizing poplar bark. This technique entails hydrolyzing biomass constituents and then condensing them within a reaction medium. Importantly, the diverse chemical composition of bark may foster the development of HS abundant in functionality.

A schematic representation of the synthetic procedure is illustrated in **Figure 1a**. AHS were synthesized across a gradient of manganese inclusion levels (0–20% of biomass weight). The reaction was performed under alkaline conditions, with the proportion of alkali that enabled neutral pH at the end of the reaction. Previous research within our group established this condition as optimal for artificial humification (Tkachenko et al., 2023). Excess alkali promotes molecular fragmentation into low-molecular-weight products, whereas insufficient alkali favors the formation of insoluble, condensed substances. Introducing $MnCl_2$ necessitated additional alkali to compensate for the rapid formation of insoluble manganese hydroxide. This adjustment maintains a final reaction pH within the favorable 7–7.2 range.

Hydrothermal treatment yielded a viscous, black slurry comprising soluble and insoluble constituents. To facilitate analysis of this complex system, components of AHS were isolated (**Fig. 1b**). Centrifugation or filtration permitted separation into liquid phase HS and humin material. Acidic precipitation further separated liquid HS into insoluble HA and soluble FA. Desalted protonated fractions required for specific analyses (e.g., NMR) were obtained *via* dialysis and solid-phase extraction. Recent investigations favor solid-phase extraction of FA isolation Bond Elut PPL cartridges (Li et al., 2016), which feature a modified non-polar styrene-divinylbenzene polymer.

Figure 1c shows a photo of the obtained samples; it can be seen that as the manganese concentration is increased, the liquid part becomes more transparent, indicating a decrease in the concentration of organic matter in it. This finding can be correlated with the reduction in the fraction of free carboxyl groups, which contribute to the solubility of AHS. The amount of available carboxyl functional groups within the samples was assessed using a calcium acetate titration method. In this approach, calcium acetate was introduced to the sample. Carboxylic acids with pKa values lower than acetic acid sequester calcium ions, forming insoluble salts. The released acetic acid could then be quantified by potentiometric titration. The carboxyl group content measured for the manganese-free AHS is 2.2 ± 0.4 mmol/g. This method selectively detects carboxyl groups predisposed to manganese binding. However, it may underestimate the total carboxyl content compared to techniques like NMR. This discrepancy can occur due to steric constraints that hinder interaction with Ca^{2+} or because of the presence of low-molecular-weight acids, such as lactic and formic acids, which do not precipitate with calcium. The proportion of the different fractions of HS was determined based on organic carbon analysis. **Table 1**

Please cite this article as: Volikov A., Schneider H., Tarakina N.V., Marzban N., Antonietti M., Filonenko S. Artificial humic substances as sustainable carriers for manganese: Development of a novel bio-based microfertilizer. Biofuel Research Journal 41 (2024) 2013-2024. DOI: 10.18331/BRJ2024.11.1.3.

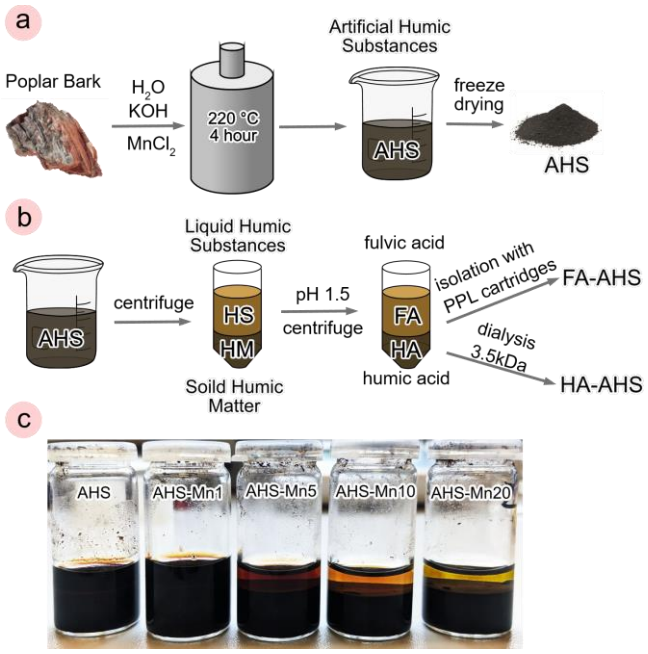

Fig. 1. A scheme of synthesis (a) and separation (b) of AHS and manganese-rich AHS and (c) visual appearance of the slurry of AHS after sedimentation.

Table 1. Content of liquid HS and their fraction in AHS based on organic carbon investigation, molar ratio of the manganese to the carboxyl groups.

Sample	C_{HS} (%)	C_{HA} (%)	C_{FA} (%)	C_{HA}/C_{FA}	n(Mn)/(AHS_{COOH}) (%)
AHS	25.2	19.1	6.1	3.1	0
AHS-Mn1	23.5	17.5	6.0	2.9	13
AHS-Mn5	19.4	13.9	5.5	2.5	65
AHS-Mn10	14.7	10.0	4.7	2.1	129
AHS-Mn20	12.3	7.9	4.4	1.8	259

shows the fractions of the AHS, as well as the ratio of manganese to carboxyl groups determined by the titration.

Table 1 shows an inverse relationship between the HS content and the content of introduced manganese, revealing possible interaction between the manganese and the carboxyl groups present in HS. Specifically, manganese content exceeding 5% appears to surpass the availability of carboxyl groups, leading to the reduced solubility of HA. Furthermore, the ratio of organic carbon in HA to FA within the solution is decreased from 3.1 (manganese absent) to 1.8 (AHS-Mn20 sample). This reduction is due to the greater abundance of functional groups in FA; these groups facilitate solubility and allow FA to remain dissolved even in the presence of manganese binding. On the contrary, HA show an increased sensitivity towards manganese presence and a greater tendency to precipitate.

GPC was used to elucidate the influence of manganese addition on the molecular weight composition of liquid HS within the fractions of HA and FA (Fig. 2). Manganese-rich synthesis conditions markedly reduce the molecular weight of HA: Mw is decreased from 11.6 KDa (AHS sample) to 3.9 KDa (AHS-Mn20 sample). Concurrently, a significant decline in the high-molecular-weight fraction of HAs is observed, with a maximum of 20 kDa for AHS-Mn20 compared to molecular weights exceeding 100 kDa in AHS. The presence of an insoluble fraction suggests that this high-molecular-weight portion of HAs forms an insoluble complex upon interaction with manganese. This hypothesis is corroborated by the almost unchanged molecular weight distribution of the FA fraction, where Mw remains 810–830 Da. Thus, manganese present in high concentrations appears to selectively bind to the high-molecular-weight fraction of HA. From an applied perspective, despite the elevated manganese content in

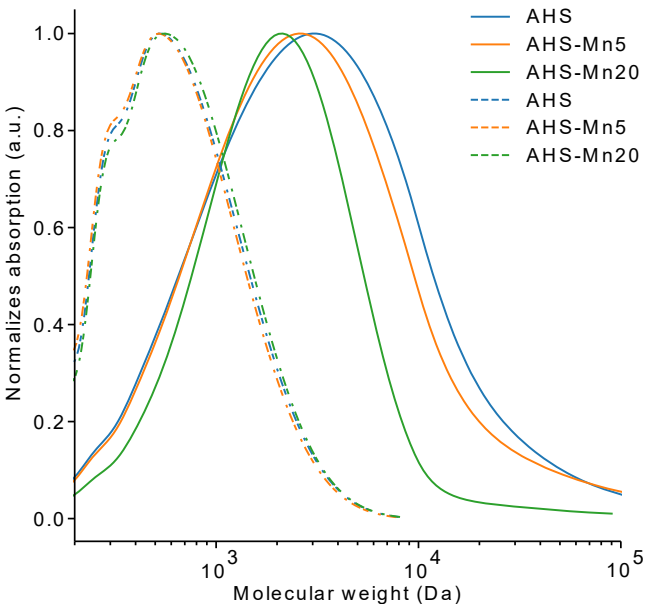

Fig. 2. Molecular weight distributions for FA (dashed lines) and HA (solid lines) of AHS and manganese-rich AHS.

AHS-Mn20 and AHS-Mn10, a significant portion of this manganese probably exists in a bound, insoluble form. In contrast, AHS-Mn5 offers substantial manganese incorporation while maintaining a high level of soluble HS amenable to transport manganese in soil, making it a potentially optimal choice.

FTIR spectroscopy was used to elucidate the functional group c ompositions of the synthesized compounds. The spectra of poplar bark and the obtained samples are shown in Figure 3. In all spectra, there is a broad absorption band at 3330–3400 cm^{-1} due to -OH stretching vibrations in phenols, alcohols, and adsorbed water. In addition, signals at 2925 and 2852 cm^{-1}, consistent with symmetric and asymmetric C-H vibrations in aliphatic groups, are common to all samples. Significant spectral differences distinguish the poplar bark spectrum from the AHS spectra in the 1500–1800 cm^{-1} wavelength region. In particular, intense peaks near 1740 cm^{-1}, attributed to C=O stretching in hemicellulose ketones and carbonyl groups, are absent in the AHS and AHS-Mn spectra. Similarly, a broad poplar bark peak in the 1580–1640 cm^{-1} region, probably due to lignin C=C vibrations, is not observed in AHS. In this region, superimposed signals at 1620 and 1400 cm^{-1} reflect asymmetric and symmetric COO^- group vibrations of calcium oxalate; XRD analysis further confirms the presence of oxalate. In manganese-free and low-manganese AHS samples (AHS-Mn), a signal near 1660 cm^{-1} is seen as the shoulder of a much more intense carboxylate peak, indicative of carboxylic acid carbonyl groups. This signal is decreased with increasing manganese concentration, possibly due to salt formation with the metals contained in the system (K, Mn, and Ca), which is also reflected in the predominance of high-intensity absorption lines of the carboxylate ion in the spectrum at 1600 and 1400 cm^{-1}.

Peaks attributed to lignin are also detected around 1500 cm^{-1} (aromatic C=C stretching) and 1250 cm^{-1} (C-O stretching). Within the AHS-Mn samples, a peak at 1300 cm^{-1} can be correlated with phenolic O-H bending. An intense signal at 1160 cm^{-1} corresponds to antisymmetric C-O-C stretching of ethers, characteristic of carbohydrates. This overlaps with a broad peak at 1030 cm^{-1} in poplar bark (characteristic of C-O stretching), which shows reduced intensity in AHS, consistent with hydrolysis in hydrothermal treatment conditions. Importantly, this signal becomes weaker relative to other peaks as the manganese content is increased, suggesting the involvement of manganese in the hydrolysis. In addition, a sharp signal at 860 cm^{-1}, indicative of C-H bending in substituted benzoic compounds, appears and intensifies with increasing manganese content; it may be caused by a change in the number of substituents during the reaction. This finding

Please cite this article as: Volikov A., Schneider H., Tarakina N.V., Marzban N., Antonietti M., Filonenko S. Artificial humic substances as sustainable carriers for manganese: Development of a novel bio-based microfertilizer. Biofuel Research Journal 41 (2024) 2013-2024. DOI: 10.18331/BRJ2024.11.1.3.

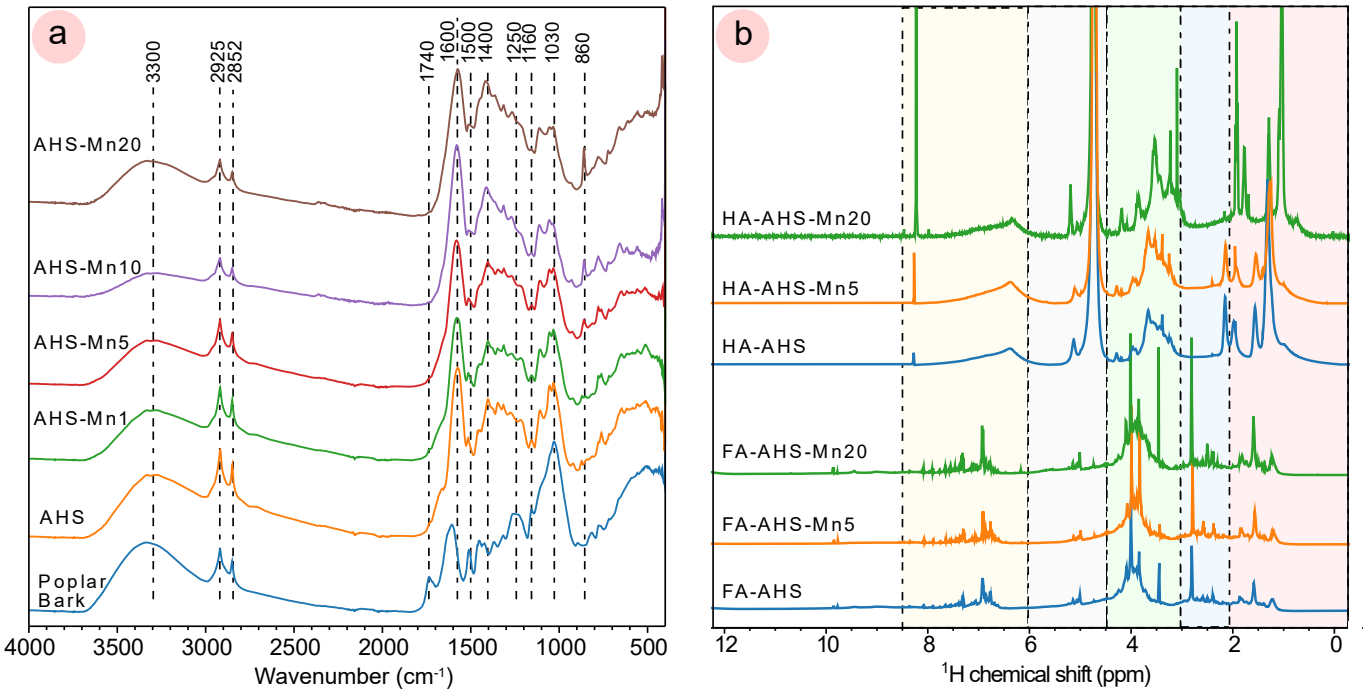

Fig. 3. FTIR spectra of Poplar Bark and AHS and manganese-rich AHS (a), H-NMR spectra of HA (b, upper, 0.3 M NaOD) and FA fractions (b, bottom, DMSO-d6) of AHS, AHS-Mn5, AHS-Mn20.

may be due to the hydrolysis of bonds between aromatic fragments in lignin in the presence of manganese, where Mn can act as a catalyst. Further research is required to fully investigate and optimize this process.

NMR spectroscopy was used to further characterize the molecular compositions of the samples. Manganese interferes with NMR spectra due to its paramagnetic properties, so samples were acidified to convert acids to protonated form, then desalted by dialysis for HA and solid phase extraction for FA. **Figure 3** displays ^{1}H-NMR spectra for FA (in DMSO-d6) and HA (in 0.3M NaOD) fractions of AHS and AHS-Mn. The 4.8 ppm signal for the HA fraction is attributed to the presence of water, which is a result of using NaOD as a solvent. Similarly, the 2.5 ppm signal for the FA fraction is due to the use of DMSO-d6 as a solvent. A 3.2 ppm signal is also observed, which is characteristic of methanol that was used during the isolation of FA and was not completely removed. The obtained spectra are consistent with those typically observed for AHS, displaying complex signal patterns. This result allows only for qualitative assessment and identification of specific spectral regions. Five main areas can be distinguished: phenolic and furan derivatives (6–8.5 ppm, yellow fill), obtained from lignin and cellulose, correspondingly; alkenes as product of condensation (4.5–6 gray fill); oxygenated aliphatic protons (3–4 ppm, green fill), which indicate dehydration intermediates of carbohydrates; signals in range 2–3 ppm (blue fill), which denote diverse organic acids, keto-acids, hydroxyl acids, and aliphatic structures below 2 ppm (red fill). These species result from the hydrothermal breakdown of primary biomass constituents and subsequent transformations that produce low-molecular-weight acids, phenolics, and various aromatics. For a detailed examination of the pathways of biomass transformation during hydrothermal humification and the corresponding NMR spectral analysis, please refer to our previous work (Tkachenko et al., 2023).

In the analysis of the NMR spectra of the HA and FA fractions, it is important to note the significantly higher content of aliphatic fragments in HA, which is demonstrated by the intense signals observed in the region below 2 ppm. This finding explains the hydrophobic nature of HA, which makes them insoluble in the acidic media used to isolate them. Additionally, more signals grouped at 3–4 ppm are observed in the region of oxygenated aliphatic protons compared to FA, indicating a wider variety of structural fragments in HA, including structural residues of sugars in their composition. The region of 6–7 ppm for HA is characterized by one broad peak belonging to the phenolic group, which is broadened by the presence of water in the sample. In contrast, FA do not exhibit this broad peak because FA samples are dissolved in DMSO. The HA spectra exhibit a peak at 8.2, which is characteristic of aldehydes derived from furfural. It is worth noting that the intensity of this peak is increased by increasing the manganese content. It is noteworthy that the intensity of this peak increased with higher manganese content. This observation suggests that manganese likely serves as a catalyst, promoting holocellulose hydrolysis to furfural derivatives.

Further analyses structural analysis of the AHS samples was performed using 2D NMR HSQC spectroscopy (**Fig. 4**). The multiplicity edited regime was employed to differentiate CH, CH_2, and CH_3 signals, providing a crucial advantage when investigating complex systems such as HS. The spectra of FA-AHS and FA-AHS-Mn20 are nearly identical, indicating that the addition of manganese has little effect on the composition of organic matter under synthesis conditions. The aliphatic region (δC/δH: 10 - 40 / 0.5 - 2 ppm) contains various methyl CH_3 and methylene CH_2 groups that are characteristic of aliphatic chains. In the region (δC/δH: 30 - 40 / 2 - 3 ppm), signals from CH_2 groups associated with the carbonyl group are observed, which may appear as a result of hydrolysis and degradation of cellulose. In the region (δC/δH: 50 - 60 / 3.5 - 4 ppm), CH_3 esters are present, which are contained in lignin and were not completely hydrolyzed during the reaction. In the oxygenated aliphatic region (δC/δH: 60-90/3-4 ppm), there are resonances from functionalized carbon chains substituted with heteroelement-containing groups, as well as from carbohydrates. This region shows an abundance of signals from intermediate and cyclic carbohydrates formed during the hydrolysis of cellulose. The region's signals (δC/δH: 105-110 / 4.5-5 ppm) can be attributed to substituted alkenes formed during the condensation reaction of different components in the system. The region (δC/δH: 110-140 / 6.5-8 ppm) contains signals from various protons belonging to aromatic compounds, such as phenols formed from the hydrolysis of lignin and furan derivatives formed from cellulose.

Please cite this article as: Volikov A., Schneider H., Tarakina N.V., Marzban N., Antonietti M., Filonenko S. Artificial humic substances as sustainable carriers for manganese: Development of a novel bio-based microfertilizer. Biofuel Research Journal 41 (2024) 2013-2024. DOI: 10.18331/BRJ2024.11.1.3.

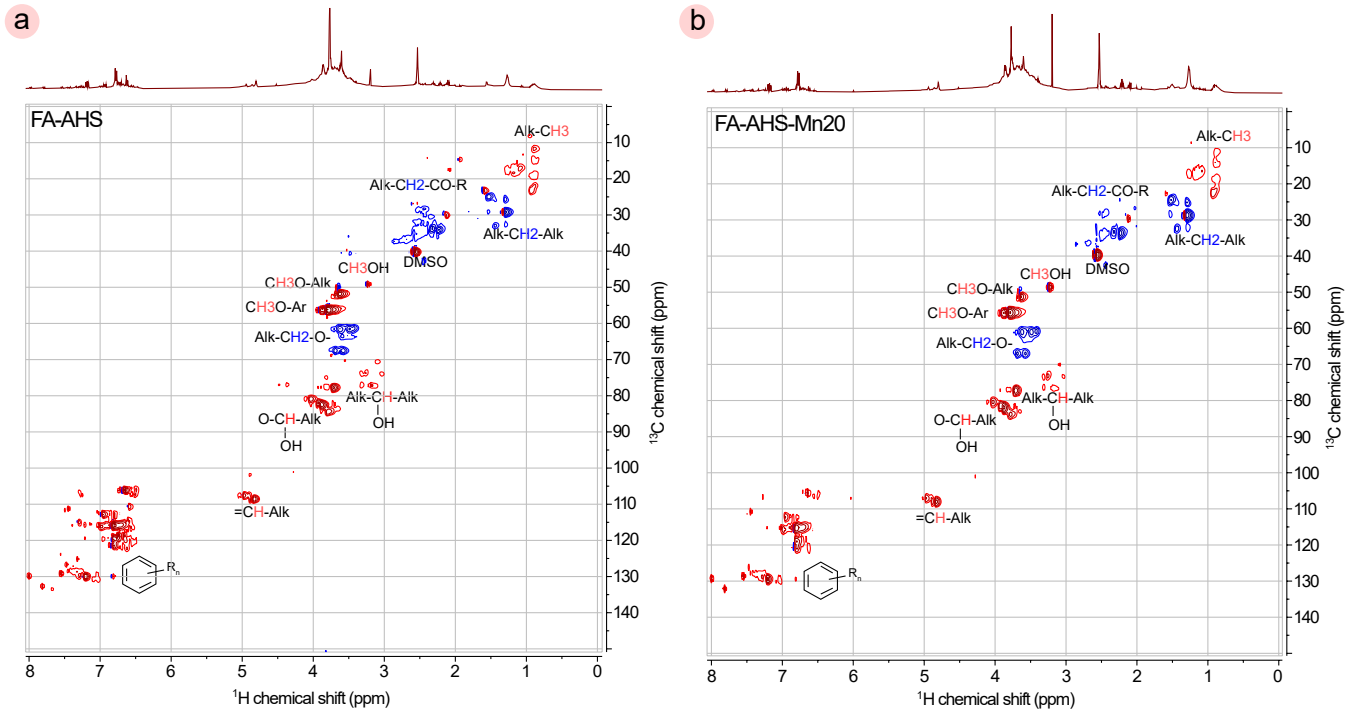

Fig. 4. ^{1}H-^{13}C HSQC NMR spectra of FA fraction of AHS (a) and manganese-rich AHS obtained in synthesis with 20% Mn added (AHS-Mn20) (b) (DMSO-d6, phase-sensitive: –CH2– opposite phase (blue) than –CH– and –CH3 (red)). The spectra were obtained on a 400 MHz NMR spectrometer with a 5 h total acquisition time.

HPLC was used to quantify low-molecular-weight organic acids and phenolic aromatics (Fig. 5), with separate analyses of the liquid and solid fractions after hydrothermal treatment. The organic acids within the solid fraction of AHS-Mn samples exhibited a pattern of initial concentration increase followed by a subsequent decrease with rising manganese content. This behavior, particularly pronounced in solid fractions of AHS-Mn1 and AHS-Mn5, is probably due to the influence of manganese compounds on hydrothermal humification. At manganese contents of 1% or 5%, soluble manganese-containing compounds are formed., which could potentially enhance biomass degradation to low-molecular-weight acids *via* homogeneous catalysis, but further investigation is required to confirm this. Conversely, concentrations of aromatic compounds showed an inverse trend. Phenol levels were significantly reduced in AHS-Mn1 and AHS-Mn5 preparations. This observation suggests that the phenols studied may bind to ionic manganese and form complexes. This effect is especially marked in the case of catechin, which is able to actively form complexes with metals, the concentration of which drops to almost zero in the case of AHS-Mn5, possibly indicating its binding in the insoluble part of humic matter.

These results show that manganese alters the course of hydrothermal humification. This influence is due to two potential mechanisms: firstly, the ability of manganese as a transition element to participate in catalytic reactions, and secondly, its propensity to form stable complexes or compounds with biomass hydrolysis products, potentially hindering certain transformations. However, at low additions of manganese (up to 5% of biomass), FTIR and NMR spectra show minimal effects. Core signals remain consistent, indicating that manganese-induced transformations affect the miscellaneous portion of the total organic matter.

3.2. Characterization of the crystallinity and morphology of manganese-rich artificial humic substances

Powder XRD was used to investigate the crystalline phases present in AHS samples synthesized from the poplar bark biomass with varying amounts of manganese (Fig. 6). XRD analysis revealed the presence of calcium oxalate ($CaC_2O_4 \cdot H_2O$, PDF-96-210-5965) in all samples, including the initial biomass, indicating its natural origin. Previous studies support the prevalence of calcium oxalate in natural plants (Li et al., 2022). This compound persists under hydrothermal treatment conditions, and this remains evident in the AHS samples. In addition, a broad signal near 2theta = 22° was present in all samples and is attributable to the signal from cellulose. This finding suggests incomplete consumption of cellulose during hydrothermal treatment under the used conditions. XRD patterns of manganese-containing samples (AHS-Mn5 and AHS-Mn20) demonstrated distinct, well-resolved peaks of sylvite (KCl, PDF-96-900-8652). This phase forms from the reaction of $MnCl_2$ and KOH during the synthesis. The remaining peaks were difficult to assign to any phases in the powder diffraction database PDF4 (Gates-Rector and Blanton, 2019); in particular, two broad peaks near 2theta =31° and =52° cannot be unambiguously matched to known manganese compounds. An increase in the intensity of these peaks with increasing manganese content suggests that the formation of the unknown phase requires the presence of manganese in the sample. One hypothesis is that these peaks arise from the interaction of calcium oxalate with manganese, possibly due to manganese incorporation into the crystal lattice. Partial substitution of calcium by manganese could both broaden and shift existing calcium oxalate peaks. However, the relatively subtle changes observed in XRD patterns imply that a significant portion of the manganese compounds probably exist in an amorphous state.

SEM analysis was used to analyze the morphology and the chemical composition at the microscale (Fig. 7a). All samples were predominantly composed of large particles 10–100 µm in diameter, which resemble the typical appearance of the solid polymer substance. In manganese-rich samples, in addition to the large polymeric particles, aggregates of small spherical particles (100–200 nm in diameter) were observed. Introducing manganese might facilitate the formation of small particles of humic substance that form aggregates and subsequently settle onto the surfaces of larger particles. Conversely, in the absence of manganese, HS appear to be more uniformly distributed without any discernable individual fragments.

Analysis of the EDX maps collected from the AHS-Mn5 sample (Fig. 7b) confirms the uniform distribution of Mn in both larger and smaller

Please cite this article as: Volikov A., Schneider H., Tarakina N.V., Marzban N., Antonietti M., Filonenko S. Artificial humic substances as sustainable carriers for manganese: Development of a novel bio-based microfertilizer. Biofuel Research Journal 41 (2024) 2013-2024. DOI: 10.18331/BRJ2024.11.1.3.

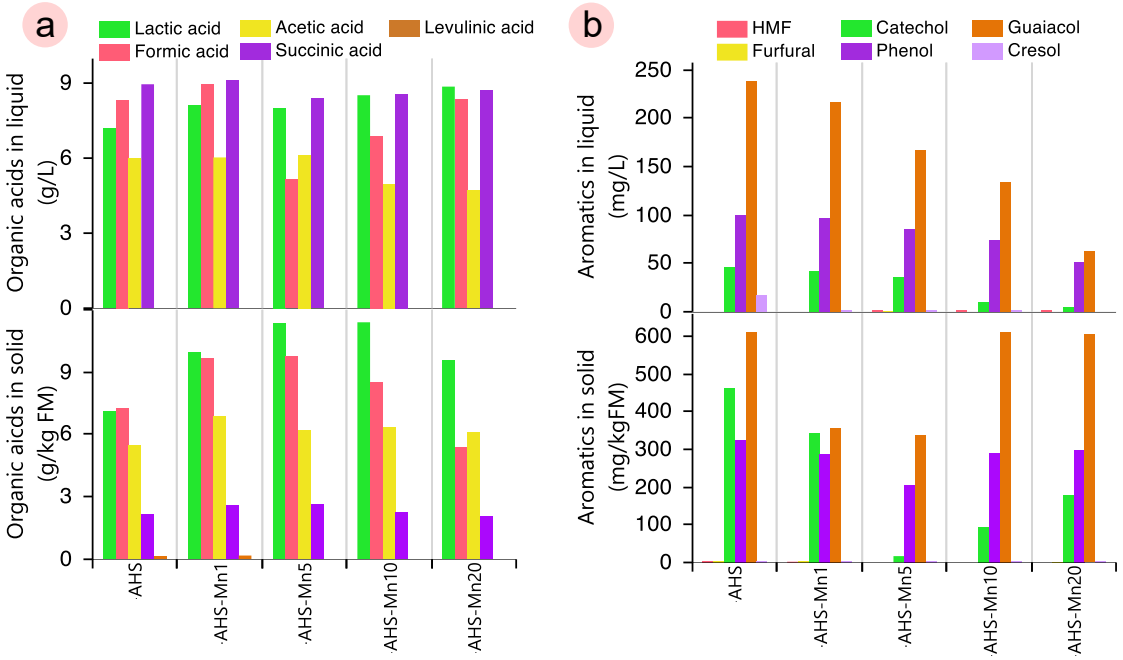

Fig. 5. Content of organic acids (a) and phenol derivatives (b) in the liquid and solid part of AHS and manganese-rich AHS determined with HPLC.

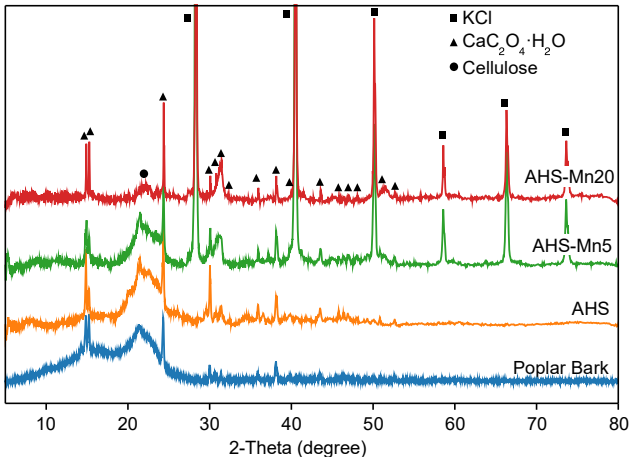

Fig. 6. X-ray powder diffraction patterns of poplar bark, AHS, and manganese-rich AHS.

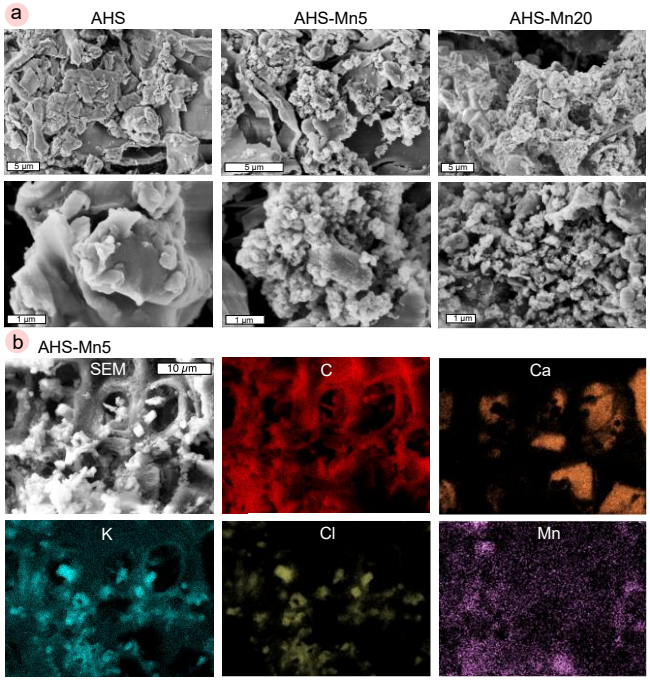

Fig. 7. (a) SEM images of AHS and manganese-rich AHS, (b) an SEM image of AHS-Mn5 and the corresponding energy dispersive X-ray maps of elemental carbon (C), calcium (Ca), potassium (K), chlorine (Cl) and manganese (Mn).

particles. In addition, in some areas of the SEM images, cubic crystals can be found, which can be assigned to sylvite (KCl) based on the distribution of EDX signals obtained from K and Cl. Calcium oxalate typically exhibits a variety of morphologies (e.g., stars, rods, and lamellae) (Thongboonkerd et al., 2006). While challenging to differentiate against the biomass background, a closer analysis of the calcium distribution indicates the presence of lamellar crystals, particularly in the central region of the SEM image (**Fig. 7b**).

Two samples (AHS-Mn5 and AHS-Mn20) were studied using STEM imaging techniques coupled with EDX analysis and electron energy loss (EEL) spectroscopy. The use of spectroscopy techniques helped to distinguish between different components in the samples. **Figure 8** shows a typical EDX spectrum obtained from the AHS-Mn20 sample. The large randomly shaped particle in the annular dark-field scanning transmission electron microscopy (ADF-STEM) image represents the product of the biomass degradation in the presence of Mn^{2+}; it contains Mn, C, O, and small amounts of Si, K, and Cl (**Fig. 8**). Smaller spherical particles (100–200 nm), an agglomerate of which is marked with white arrows on **Figure 8**, mainly contain Ca, Mn and O; it is worth mentioning that these particles are also present in the perimeter of the large particle as well as randomly distributed on its surface. The lamellar-shaped particle on the right side of

Please cite this article as: Volikov A., Schneider H., Tarakina N.V., Marzban N., Antonietti M., Filonenko S. Artificial humic substances as sustainable carriers for manganese: Development of a novel bio-based microfertilizer. Biofuel Research Journal 41 (2024) 2013-2024. DOI: 10.18331/BRJ2024.11.1.3.

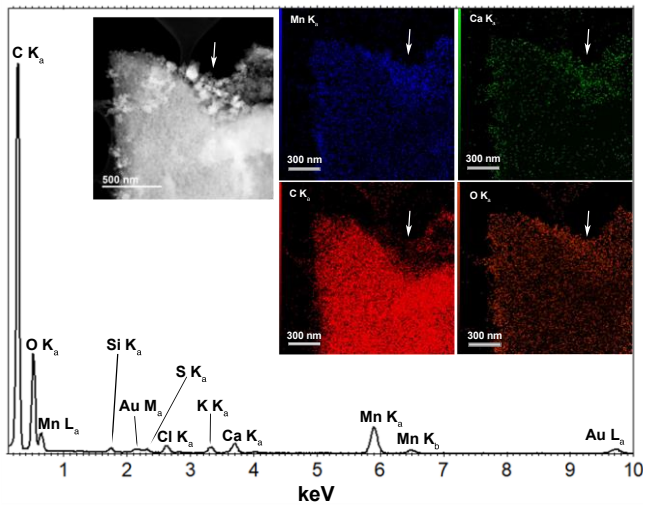

Fig. 8. EDX spectrum of the AHS-Mn-20 sample obtained from the full area of the ADF-STEM image, shown in the inset. Corresponding EDX maps were obtained using K_α - lines of Mn, Ca, C, and O. White arrows indicate the area with small particles (100–200 nm), which mainly contain Ca, Mn, and O.

the annular dark field (ADF)-STEM image contains a high amount of Ca and, most probably, corresponds to the crystalline Ca oxalate present in all samples (see **Fig. 6**).

The large particles obtained from biomass in the presence of 5% and 20% of Mn^{2+} have random shapes and the typical appearance of amorphous polymers (**Figs. 9a and b**). The carbon K-lines on the corresponding EEL spectra have a shape characteristic of amorphous polymers with a weak π*-peak and a broad σ*-peak. Ca $L_{3,2}$ and Mn $L_{3,2}$ lines are present on EEL spectra from both samples. The peak position of the Mn $L_{3,2}$ – edge is at 641 eV with no additional peaks at ~643 eV, suggesting that the majority of the Mn-ions in the AHS-Mn20 sample have oxidation state 2+ (inset to **Fig. 9**). In the case of AHS-Mn5, we were not able to analyze the Mn-edge due to the low signal-to-noise ratio on the spectra. The presence of manganese in the 2+ oxidation state can be explained by the redox properties of AHS (Yang et al., 2023). During the synthesis of AHS, electron-rich (i.e., reduced) groups, such as phenolic groups, are formed, and they are able to prevent manganese oxidation.

3.3. Bioassay

The obtained data suggest that manganese primarily exists in the +2 oxidation state within an amorphous matrix. This form likely facilitates plant uptake, as manganese is primarily absorbed as free divalent Mn^{2+} cations from the growth medium and translocated from roots to shoots (Alejandro et al., 2020). This study examined the bioavailability of manganese for hydroponically grown cucumber plants (*Cucumis sativus L.*), a species known for its sensitivity to manganese concentration (Crawford et al., 1989). We used a modified Hoagland medium adjusted to pH 8 to simulate alkaline soil conditions, while alkaline soils can limit manganese bioavailability due to the formation of insoluble hydroxides and oxyhydroxides, and for them, this problem is particularly acute. To distinguish the effects of AHS, we add separately AHS combined with a manganese salt and the pre-prepared AHS-Mn complex into the medium. Iron levels were monitored to assess the influence of AHS on the transport of other metals. The findings are summarized in **Figure 10**.

The data for manganese (**Fig. 10a**) demonstrated the superior efficacy of AHS-Mn5 compared to the manganese salt alone. Furthermore, combining manganese salt with unmodified AHS resulted in a notable, albeit reduced, increase in manganese bioavailability. Higher quantities of AHS were found to facilitate manganese transport within the system, likely due to AHS interacting with manganese hydroxide and enhancing its solubility, promoting delivery to plants. Higher quantities of AHS were found to facilitate manganese transport within the system, likely due to AHS

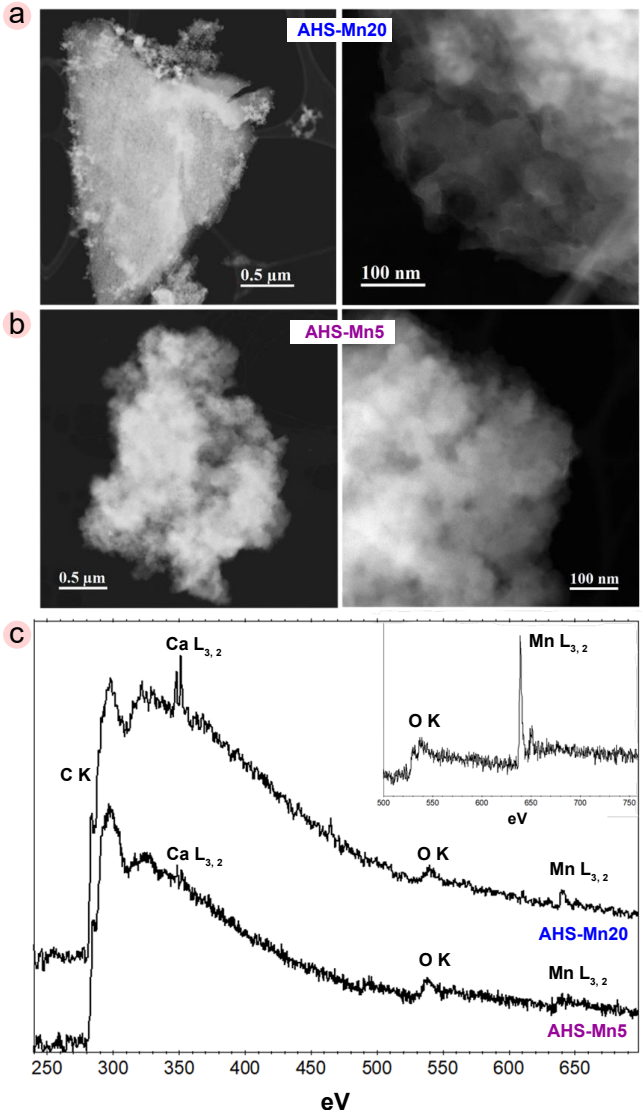

Fig. 9. ADF-STEM images of manganese-rich artificial (a) AHS-Mn5 and (b) AHS-Mn20 samples, showing the overview and enlargement of the large particles obtained from the biomass degradation; (c) corresponding electron energy loss spectra. The inset shows the spectrum obtained from AHS-Mn20 at 0.1 eV/channel dispersion, highlighting O K and Mn $L_{3,2}$ edges.

interacting with manganese hydroxide and enhancing its solubility, promoting delivery to plants. This interpretation is reinforced by the analysis of iron content (**Fig. 10b**). The results showed a significant increase in iron accumulation after the introduction of AHS, highlighting their ability to transport metals.

The data show that in all cases, a sufficient amount of manganese (more than 20 mg/kg according to Broadley et al., 2012) was obtained, and deficiency only occurred when no manganese was added. This result suggests that both simple salts and AHS-Mn are equally effective in controlling manganese deficiency. However, it is essential to consider other disadvantages of conventional fertilizers, such as seepage into groundwater, a concern largely mitigated by the use of HS. Additionally, the data obtained for iron indicates a positive contribution of HS to the transport of micronutrients.

Although AHS-Mn shows potential for delivering manganese, further investigation is necessary. Conducting laboratory soil studies is crucial for evaluating interactions with mineral and organic phases, as well as assessing the impact of microbiomes on manganese transport and transformation, as

Please cite this article as: Volikov A., Schneider H., Tarakina N.V., Marzban N., Antonietti M., Filonenko S. Artificial humic substances as sustainable carriers for manganese: Development of a novel bio-based microfertilizer. Biofuel Research Journal 41 (2024) 2013-2024. DOI: 10.18331/BRJ2024.11.1.3.

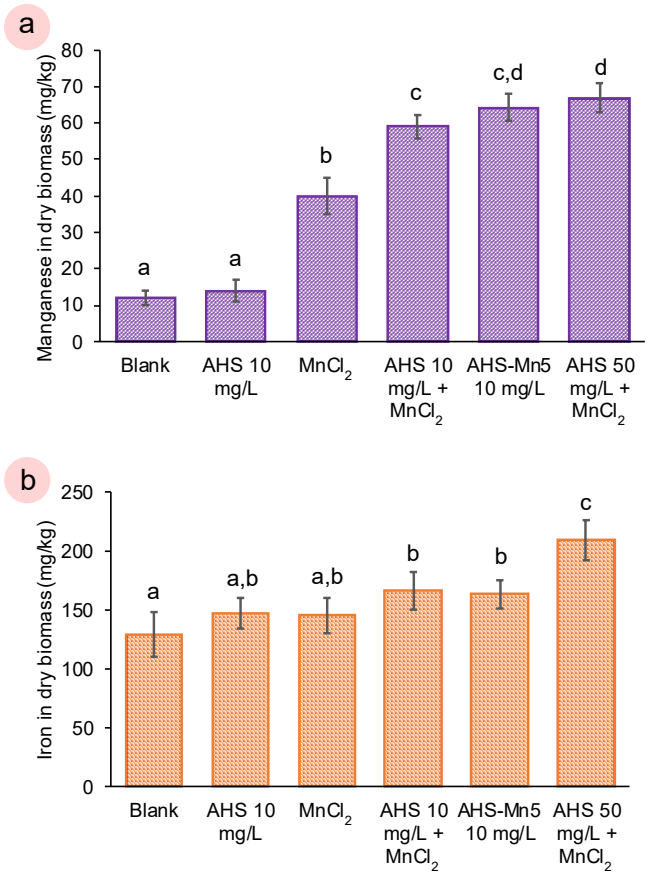

Fig. 10. Manganese (a) and iron (b) content (% blank) in dried plants treated with AHS (10 m/L), $MnCl_2$, AHS (10 mg/L) with $MnCl_2$, manganese-rich AHS with 5% Mn content at synthesis (AHS-Mn5) (10 mg/L), AHS (50 mg/L) with $MnCl_2$. Error bars represent standard deviation (n = 10). Values with different letters are significantly different at $p < 0.05$ by one-way ANOVA test.

observed in Khoshru et al. (2023). Long-term field trials are necessary to validate the effectiveness of these compounds under natural conditions. Also, this research suggests the further possibility of using AHS-based microfertilizers to incorporate other essential micronutrients, such as zinc and iron, using the same synthesis principles.

4. Conclusions

This study demonstrates a novel approach for the production of micronutrient fertilizers through the hydrothermal humification of biomass, in which the incorporation of metal salts, specifically manganese, directly influences the composition of the resulting compounds. We found that manganese alters hydrothermal humification, highlighting the need for careful formulation to achieve specific downstream applications. Notably, manganese forms amorphous structures within the AHS, exhibiting an even distribution and a primarily plant-available Mn(II) oxidation state. Biotests on cucumber plants confirmed the superior efficiency of AHS-Mn5 in boosting manganese bioavailability compared to the use of a bare manganese salt, $MnCl_2$. Additionally, AHS could facilitate iron uptake, thus demonstrating their broader role in enhancing metal transport mechanisms within plants. While excessive manganese concentrations can reduce AHS solubility, the AHS-Mn5 formulation (5% manganese content) successfully balanced effective manganese incorporation, maintaining sufficient AHS solubility. This formulation shows a significant potential to be used in humic-based fertilizers, which can provide solubilized manganese compounds required by plants. Overall, our findings introduce a promising new avenue for tailoring micronutrient fertilizer production *via* hydrothermal humification technology, utilizing readily available biomass for increased agricultural efficiency.

Acknowledgements

This research did not receive any specific grant from funding agencies in the public, commercial, or not-for-profit sectors. A. V., H. S., N. T., S. F., and M. A. gratefully acknowledge the Max Planck Society for financial support. N. M. thanks the analytical chemistry group (Leibniz Institute of Agricultural Engineering and Bioeconomy) for their expertise and support with the analytical techniques.

References

[1] Alejandro, S., Höller, S., Meier, B., Peiter, E., 2020. Manganese in plants: from acquisition to subcellular allocation. Front. Plant Sci. 11, 300.
[2] Alloway, B.J., 2008. Micronutrients and crop production: an introduction, in: Micronutrient Deficiencies in Global Crop Production. Springer. 1-39.
[3] Ampong, K., Thilakaranthna, M.S., Gorim, L.Y., 2022. Understanding the role of humic acids on crop performance and soil health. Front. Agron. 4, 848621.
[4] Andresen, E., Peiter, E., Küpper, H., 2018. Trace metal metabolism in plants. J. Exp. Bot. 69, 909-954.
[5] Boiteau, R.M., Shaw, J.B., Pasa-Tolic, L., Koppenaal, D.W., Jansson, J.K., 2018. Micronutrient metal speciation is controlled by competitive organic chelation in grassland soils. Soil Biol. Biochem. 120, 283-291.
[6] Broadley, M., Brown, P., Cakmak, I., Rengel, Z., Zhao, F., 2012. Chapter 7-function of nutrients: micronutrients, in: marschner's mineral nutrition of higher plants. Elsevier, pp. 191-248.
[7] Chakraborty, M., Chakraborty, D., Mondal, P., Paul, R., 2021. Micronutrient deficiency stress in soils of India: tackling it to alleviate hidden hunger, in: Rakshit, A., Singh, S.K., Abhilash, P.C., Biswas, A. (Eds.), Soil Science: Fundamentals to Recent Advances. Springer Singapore, Singapore. 801-821.
[8] Chen, Y., 1996. Chapter 13-organic matter reactions involving micronutrients in soils and their effect on plants, in: Humic Substances in Terrestrial Ecosystems. Elsevier. 507-529.
[9] Cieschi, M.T., Polyakov, A.Y., Lebedev, V.A., Volkov, D.S., Pankratov, D.A., Veligzhanin, A.A., Perminova, I.V., Lucena, J.J., 2019. Eco-Friendly iron-humic nanofertilizers synthesis for the prevention of iron chlorosis in soybean (glycine max) grown in calcareous soil. Front. Plant Sci. 10, 413.
[10] Crawford, T.W., Stroehlein, J.L., Kuehl, R.O., 1989. Manganese and rates of growth and mineral accumulation in cucumber. J. Am. Soc. Hort. Sci. 114(2), 300-306.
[11] Dhaliwal, S.S., Sharma, V., Shukla, A.K., Verma, V., Kaur, M., Alsuhaibani, A.M., Gaber, A., Singh, P., Laing, A.M., Hossain, A., 2023. Minerals and chelated-based manganese fertilization influences the productivity, uptake, and mobilization of manganese in wheat (Triticum aestivum L.) in sandy loam soils. Front. Plant Sci. 14, 1163528.
[12] Dimkpa, C.O., Bindraban, P.S., 2016. Fortification of micronutrients for efficient agronomic production: a review. Agron. Sustainable Dev. 36, 7.
[13] Fang, S., Xue, J., Tang, L., 2007. Biomass production and carbon sequestration potential in poplar plantations with different management patterns. J. Environ. Manage. 85(3), 672-679.
[14] Fortier, J., Truax, B., Gagnon, D., Lambert, F., 2016. Potential for hybrid poplar riparian buffers to provide ecosystem services in three watersheds with contrasting agricultural land use. Forests. 7(2), 37.
[15] Gates-Rector, S., Blanton, T., 2019. The powder diffraction file: a quality materials characterization database. Powder Diffr. 34(4), 352-360.
[16] Gomollón-Bel, F., 2021. Breakthroughs for a circular, climate-neutral future. Chem. Int. 43(4), 13-20.
[17] Gupta, A.P., 2005. Micronutrient status and fertilizer use scenario in India. J. Trace Elem. Med. Biol. 18(4), 325-331.

Please cite this article as: Volikov A., Schneider H., Tarakina N.V., Marzban N., Antonietti M., Filonenko S. Artificial humic substances as sustainable carriers for manganese: Development of a novel bio-based microfertilizer. Biofuel Research Journal 41 (2024) 2013-2024. DOI: 10.18331/BRJ2024.11.1.3.

[18] Hajiboland, R., 2012. Effect of Micronutrient Deficiencies on Plants Stress Responses, in: Ahmad, P., Prasad, M.N.V. (Eds.), Abiotic Stress Responses in Plants: Metabolism, Productivity and Sustainability. Springer New York, New York, NY. 283-329.
[19] Hoagland, D.R., Arnon, D.I., 1950. The water-culture method for growing plants without soil. Circ. Calif. Agric. Exp. Stat. 347(2nd), 32.
[20] Jeong, C.Y., Park, C.W., Kim, J.G., Lim, S.K., 2007. Carboxylic content of humic acid determined by modeling, calcium acetate, and precipitation methods. Soil Sci. Soc. Am. J. 71(1), 86-94.
[21] Khoshru, B., Mitra, D., Nosratabad, A.F., Reyhanitabar, A., Mandal, L., Farda, B., Djebaili, R., Pellegrini, M., Guerra-Sierra, B.E., Senapati, A., Panneerselvam, P., Mohapatra, P.K.D., 2023. Enhancing manganese availability for plants through microbial potential: a sustainable approach for improving soil health and food security. bacteria. 2(3), 129-141.
[22] Li, P., Liu, C., Luo, Y., Shi, H., Li, Q., PinChu, C., Li, X., Yang, J., Fan, W., 2022. Oxalate in plants: metabolism, function, regulation, and application. J. Agric. Food Chem. 70(51), 16037-16049.
[23] Li, Y., Harir, M., Lucio, M., Kanawati, B., Smirnov, K., Flerus, R., Koch, B.P., Schmitt-Kopplin, P., Hertkorn, N., 2016. Proposed guidelines for solid phase extraction of suwannee river dissolved organic matter. Anal. Chem. 88(13), 6680-6688.
[24] López-Rayo, S., Lucena, S., Lucena, J.J., 2014. Chemical properties and reactivity of manganese chelates and complexes in solution and soils. Z. Pflanzenernähr. Bodenk. 177(2), 189-198.
[25] Lumactud, R.A., Gorim, L.Y., Thilakarathna, M.S., 2022. Impacts of humic-based products on the microbial community structure and functions toward sustainable agriculture. Front. Sustainable Food Syst. 6, 977121.
[26] Lupoi, J.S., Singh, S., Parthasarathi, R., Simmons, B.A., Henry, R.J., 2015. Recent innovations in analytical methods for the qualitative and quantitative assessment of lignin. Renew. Sust. Energy Rev. 49, 871-906.
[27] MacCarthy, P., 2001. The principles of humic substances. Soil Sci. 166(11), 738-751.
[28] Nieder, R., Benbi, D.K., Reichl, F.X., 2018. Microelements and their role in human health, in: Soil Components and Human Health. Springer Netherlands, Dordrecht. 317-374.
[29] Norvell, W.A., Lindsay, W.L., 1969. Reactions of EDTA complexes of Fe, Zn, Mn, and Cu with soils. Soil Science Soc. Am. J. 33(1), 86-91.
[30] Rashed, M., Hoque, T., Jahangir, M., Hashem, M., 2021. Manganese as a micronutrient in agriculture: crop requirement and management. J. Environ. Sci. Nat. Resour. 12, 225-242.
[31] Rengel, Z., 2015. Availability of Mn, Zn and Fe in the rhizosphere. J. Soil Sci. Plant Nutr.15(2), 397-409.
[32] Reuter, D.J., Alston, A.M., McFarlane, J.D., 1988. Occurrence and Correction of Manganese Deficiency in Plants, in: Graham, R.D., Hannam, R.J., Uren, N.C. (Eds.), Manganese in Soils and Plants: Proceedings of the International Symposium on `Manganese in Soils and Plants' Held at the Waite Agricultural Research Institute. The University of Adelaide, Glen Osmond, South Australia, August 22-26, 1988 as an Australian Bicentennial Event. Springer Netherlands, Dordrecht. 205-224.
[33] Saquee, F.S., Diakite, S., Kavhiza, N.J., Pakina, E., Zargar, M., 2023. The efficacy of micronutrient fertilizers on the yield formulation and quality of wheat grains. Agronomy. 13(2), 566.
[34] Schmidt, S.B., Husted, S., 2019. The Biochemical properties of manganese in plants. Plants 8(10), 381.
[35] Sorkina, T.A., Polyakov, A.Yu., Kulikova, N.A., Goldt, A.E., Philippova, O.I., Aseeva, A.A., Veligzhanin, A.A., Zubavichus, Y.V., Pankratov, D.A., Goodilin, E.A., Perminova, I.V., 2014. Nature-inspired soluble iron-rich humic compounds: new look at the structure and properties. J. Soils Sediments. 14, 261-268.
[36] Thongboonkerd, V., Semangoen, T., Chutipongtanate, S., 2006. Factors determining types and morphologies of calcium oxalate crystals: molar concentrations, buffering, pH, stirring and temperature. Clin. Chim. Acta. 367(1-2), 120-131.
[37] Tkachenko, V., Marzban, N., Vogl, S., Filonenko, S., Antonietti, M., 2023. Chemical insights into the base-tuned hydrothermal treatment of side stream biomasses. Sustainable Energy Fuels. 7(3), 769-777.
[38] Vangeel, T., Neiva, D.M., Quilhó, T., Costa, R.A., Sousa, V., Sels, B.F., Pereira, H., 2023. Tree bark characterization envisioning an integrated use in a biorefinery. Biomass Convers. Biorefin. 13, 2029-2043.
[39] Yang, F., Antonietti, M., 2020. Artificial Humic Acids: sustainable materials against Climate Change. Adv. Sci.7(5), 1902992.
[40] Yang, F., Fu, Q., Antonietti, M., 2023. Anthropogenic, carbon-reinforced soil as a living engineered material. Chem. Rev. 123(5), 2420-2435.
[41] Zanin, L., Tomasi, N., Cesco, S., Varanini, Z., Pinton, R., 2019. Humic substances contribute to plant iron nutrition acting as chelators and biostimulants. Front. Plant Sci. 10, 675.

Alexander Volikov is a postdoctoral researcher at the Max Planck Institute of Colloids and Interfaces in Potsdam, Germany. After receiving his Ph.D. in Environmental Chemistry from Lomonosov Moscow State University in 2018, he continued his research there until 2022, specializing in the properties and applications of natural humic substances. He joined the Max Planck Institute in 2023, shifting his focus to artificial humic substances. His research interests include the structure and properties of humic substances, their interactions with minerals and the microbiome, and both practical and theoretical investigations into humification processes.

Helen Schneider has a Master's degree in Chemical Engineering for Energy and the Environment from KTH Royal Institute of Technology, Sweden and a Bachelor`s Degree from the University of Twente, the Netherlands. She has a Ph.D. in chemistry in 2023 at Potsdam University on topic Reactive eutectic media based on ammonium formate for the valorization of bio-sourced materials. During her Ph.D. program she worked as a researcher in the Sustainable Solvents Group at the Max Planck Institute of Colloids and Interfaces, Germany.

Please cite this article as: Volikov A., Schneider H., Tarakina N.V., Marzban N., Antonietti M., Filonenko S. Artificial humic substances as sustainable carriers for manganese: Development of a novel bio-based microfertilizer. Biofuel Research Journal 41 (2024) 2013-2024. DOI: 10.18331/BRJ2024.11.1.3.

Nadezda V. Tarakina leads the Electron Microscopy research group at the Max Planck Institute of Colloids and Interfaces, Potsdam (Germany). After completing her PhD in Chemistry at the Institute of Solid State Chemistry in Yekaterinburg (Russia), she performed research in Belgium, Germany, Russia, Sweden and the UK, combining different scattering techniques and transmission electron microscopy to study highly-disordered structures. She got her Habilitation in Experimental Physics from the University of Wuerzburg (Germany) in 2020. Her main research interest lies in developing approaches for characterising soft functional materials and their interfaces with hard matter at the nanoscale using electron microscopy techniques. She has authored over 140 peer-review journal papers.

Markus Antonietti is the Materials Chemistry Director of the Max Planck Institute of Colloids and Interfaces in Potsdam-Golm. He is an expert in polymers and covalent materials and has focused his attention in the last years to the fields of green chemistry, and sustainable materials, but also to the new global cycles of energy, food, water, and CO_2 constituting the Anthropocene. In his free time, he enjoys cooking and performing in a rock band.

Nader Marzban is currently working as a full-time researcher at the Leibniz Institute for Agricultural Engineering and Bioeconomy (ATB), Potsdam, Germany, with a focus on the thermochemical conversion of biomass, specifically through hydrothermal processes. He completed his PhD in 2023 on hydrothermal carbonization, humification, and fulvification of agricultural residues under the supervision of Dr. Judy Libra and Prof. Susanne Rotter from the Technical University of Berlin. During his PhD, he conducted a research stay at the Max Planck Institute of Colloids and Interfaces, department of colloid chemistry, Potsdam, Germany. During his stay, he learned the chemistry behind the hydrothermal carbonization and humification of various biomasses under the supervision of Dr. Svitlana Filonenko and Prof. Markus Antonietti. He has published 18 research papers in peer-reviewed journals. Within the 'Saving a Tree' project, he collaborated with a team to produce and apply artificial humic substances, successfully preserving a 160-year-old beech tree in historical Park Sanssouci, Potsdam, Germany.

Svitlana Filonenko is leading a Sustainable Solvents for Green Processes group at Max Planck Institute of Colloids and Interfaces. She has her PhD degree in Physical Chemistry from Yuriy Fedkovych Chernivtsi National University. She worked at National Academy of Science of Ukraine and made her postdoc at Aalto University. Her research interest are on sustainable and green chemistry, biopolymers and materials science.

Please cite this article as: Volikov A., Schneider H., Tarakina N.V., Marzban N., Antonietti M., Filonenko S. Artificial humic substances as sustainable carriers for manganese: Development of a novel bio-based microfertilizer. Biofuel Research Journal 41 (2024) 2013-2024. DOI: 10.18331/BRJ2024.11.1.3.